The use of light in cancer immunotherapy

Kleinovink, E.J.W.

Chapter 4

Vaccine tracking by in vivo near-infrared fluorescence imaging of emulsified peptide antigen

Jan Willem Kleinovink, Laura Mezzanotte, Henrik Gold, Nico Meeuwenoord, Luis J. Cruz, Alan B. Chan, Cornelis J.M. Melief, Hermen S. Overkleeft, Marieke F. Fransen, Clemens Löwik, Ferry Ossendorp

Manuscript in preparation

Abstract

Information on the fate of vaccines after *in vivo* administration may help optimize vaccination strategies. Optical imaging is a non-invasive visualization method capable of locating and quantifying light-producing molecules in vivo, which can be applied for vaccine visualization. We conjugated synthetic peptide vaccines to the near-infrared (NIR) fluorescent dye NIRD1. Using a NIRD1-labeled peptide of the OVA model antigen, we showed the feasibility of visualizing vaccines at the injection site and local lymph nodes. Distinct kinetics of different vaccine formulations were well-identified by live NIR fluorescence imaging. Small-droplet Montanide water-in-oil emulsions prepared by a syringe extrusion (SE) method showed remarkably slower vaccine kinetics than Vortex-prepared emulsions with larger droplets, which was visualized at the injection site and in draining lymph nodes. Differential vaccine drainage to lymph nodes was reflected in the ability to prime vaccine-specific CD8 T cells in local vaccine-draining lymph nodes, whereas systemic T cell levels were not significantly different. In conclusion, we have developed a NIR fluorescence imaging protocol for visualization of the fate of vaccines, which can be used to optimize vaccination strategies for several applications such as infectious disease and cancer.

Introduction

Immunotherapy of cancer aims to induce or enhance immune responses against tumors. Immune recognition can involve a variety of immune cells, but CD8 T cells are crucial immune cells capable of inducing tumor cell death through the delivery of cytotoxic T cell effector molecules. T cells recognize peptide epitopes presented in MHC molecules on the surface of target cells, and recent literature has shown T cell recognition of tumor cells driven by neo-epitopes in mutated cellular proteins (1–3). Indeed, highly mutated types of human cancer such as melanoma and lung cancer show higher numbers of neo-epitopes, correlating with a stronger immune recognition and in particular with the presence of T cells inside the tumor (4–6). Immunotherapy with immunomodulatory antibodies enhancing existing T cell responses has shown promising clinical results in patients with highly mutated and T cell-infiltrated tumors (7–9). Therapeutic vaccination is a form of cancer immunotherapy aiming to induce T cell responses by providing an exogenous source of tumor-specific antigen. The delivery of minimal peptide epitopes of tumor antigens results in direct binding to MHC molecules on any nucleated cell, resulting in T cell anergy due to antigen presentation in the absence of co-stimulatory signals. To restrict vaccine antigen presentation to professional APCs capable of priming functional T cells, the concept of synthetic long peptide (SLP) vaccines was established, which require antigen processing by professional APCs to create the MHC-binding epitope (10,11). Preclinical studies indicated that SLP vaccination may not only be applied in virally induced cancer by vaccinating with viral epitopes widely shared among individuals, both also by using individual unique neo-epitopes as a therapeutic peptide vaccine (12–14). Clinical application of SLP vaccination using a series of overlapping peptides covering the E6 and E7 oncoproteins of human papillomavirus 16 (HPV16) has shown promising results in patients with pre-malignant HPV16-induced gynecological lesions, but failed to induce strong responses in patients with established HPV16+ tumors despite the presence of vaccine-induced T cell responses (15–17). Mouse studies combining SLP vaccination with chemotherapy or photodynamic therapy have suggested combination therapy to improve the limited efficacy of SLP vaccination against advanced cancer (18,19). In addition, the efficacy of SLP vaccination as such may be improved, for example in terms of peptide formulation and routing. For instance, the fate of the vaccine peptides after injection is currently largely unknown, which could be addressed by live vaccine visualization techniques. Near-infrared (NIR) fluorescent dyes are very suitable for in vivo optical imaging studies due to their high excitation and emission wavelength, enhancing tissue penetration of the fluorescence signal (20–23). The widely used and clinically approved NIR dye Indocyanine Green (ICG) has

good optical properties as a standalone dye but is less suitable for conjugation to biomolecules (24,25). In this preclinical study, we labeled a model SLP vaccine with the novel NIR fluorescent dye NIRD1 to establish a fluorescence-based imaging platform for live SLP visualization and quantification. We visualized the vaccine at the injection site and draining lymph nodes and correlated vaccine kinetics to functionality. In conclusion, this study shows that NIR fluorescence imaging of vaccines is feasible and provides detailed information on vaccine kinetics, which can be used to optimize therapeutic vaccination strategies.

Materials and Methods

Mice and cell lines

Wildtype C57BL/6 mice and BALB/c nude mice were obtained from Charles River Laboratories (France). Albino B6 mice (tyrosinase-deficient immunocompetent C57BL/6 mice) and OT-I mice ($OVA_{257-264}$ (SIINFEKL)-specific T cell receptor-transgenic mice of C57BL/6 background) were bred in the animal breeding facility of the Leiden University Medical Center, the Netherlands. All experiments were approved by the animal ethical committee of Leiden University. D1 is a dendritic cell line and B3Z is a T cell hybridoma expressing beta-galactosidase upon presentation of its cognate antigen SIINFEKL, both are of C57BL/6 background and were used as described elsewhere (26). Cells were assured to be free of rodent viruses and *Mycoplasma* by PCR analysis.

Synthetic long peptide vaccines

For vaccine tracking experiments, the near-infrared (NIR) fluorescent dye NIRD1 was conjugated to synthetic long peptides using an aminohexanoid acid (Ahx) linker. This NIRD1-Ahx construct, amounting to approximately 1 kDa, was used to label the OVA SLP (DEVSGLEQLESIINFEKLAAAAAK). The purity of NIR-SLP conjugate preparations was visualized by Odyssey Imager (LI-COR) after tricine gel electrophoresis as described elsewhere (27). For *in vivo* vaccine tracking experiments, the NIR-SLP was injected subcutaneously in the tail-base of the mice in a volume of 100 µL, formulated in PBS or in Montanide emulsions consisting of a 1:1 ratio of a vaccine-containing PBS fraction and the mineral oil Montanide ISA 51 (Seppic). Vortex emulsions were prepared by vortexing the mixture for 30 minutes at room temperature. Syringe Extrusion emulsions were prepared by syringe extrusion of the PBS-Montanide mixture using two 1 mL syringes (Codan) connected to a three-way stopcock (Braun Discofix C3), using a protocol of 40 slow passages through the stopcock in 20 seconds followed by 160 passages at full speed. Dosing and formulation are indicated in the Figures legends.

NIR Fluorescence imaging

For live *in vivo* imaging, vaccinated mice were anaesthetized by isoflurane inhalation on the indicated time points. NIR fluorescent signals were measured by IVIS Spectrum (PerkinElmer) using excitation for 2 seconds at 745 nm and measuring the emission in the 840 nm filter, with Field Of View C and medium binning. Accompanying LivingImage software (Caliper Life Sciences) was used for data analysis. Signal quantification in specific regions of interest (ROI) was performed by using fixed-size ROIs throughout the experiments. Figures show the fluorescent signal as the Total Radiant Efficiency (TRE), expressed in (photons/second)/(μW/cm²) or as a percentage of the TRE at the start of the experiment.

Adoptive T cell transfer and T cell flow cytometry

For adoptive transfer of OVA SLP-specific OT-I CD8 T cells, the spleen of OT-I mice was harvested and mashed on 70 μm cell strainers (BD Biosciences) to create single-cell suspensions, followed by erythrocyte lysis and CD8 T cell isolation using a negative magnetic selection kit (BD). Adoptive transfer consisted of $1*10^6$ purified CD8 OT-I cells injected intravenously in 200 μL PBS in the tail vein. On indicated time points after transfer, the spleen and/or lymph nodes of recipient mice were harvested, mashed and deprived of erythrocytes, stained for CD3ε, CD8β and the OT-I congenic marker CD90.1, and analyzed by flow cytometry (BD LSR-II). To visualize OT-I proliferation, OT-I cells were labeled with the fluorescent dye carboxyfluorescein succinimidyl ester (CFSE) that is distributed among daughter cells upon cellular proliferation, reducing the fluorescence intensity per cell, which can be visualized by flow cytometry. To measure the HPV SLP-induced endogenous CD8 T cell response, venous blood samples were taken from the tail vein 8 days after vaccination. After erythrocyte lysis of the blood samples, the tumor-specific CD8 T cell response was determined by flow cytometry analysis after staining of the cells with fluorescently labeled antibodies against CD3ε, CD8β, and with 7-AAD and APC-conjugated tetramers (own production) binding the H-2Db RAHYNIVTF complex on the CD8 T cell.

Statistical analysis

Statistical analysis was performed using GraphPad Prism version 7.0 software. Data are shown as the mean ± SEM for each group, and comparison of groups was performed by two-tailed Student's t-test. Statistical differences were considered significant at $p < 0.05$.

Results and Discussion

Subcutaneously injected peptide vaccines drain to lymph nodes

In order to track the fate of antigen vaccines after vaccination, we used the near-infrared (NIR) fluorescent dye NIRD1 to label a model SLP of the chicken ovalbumin (OVA) CD8 T cell epitope SIINFEKL, creating conjugated NIR-OVASLP. To validate NIR fluorescence as a measure of vaccine presence, we tested whether no unbound NIRD1 dye was present in the conjugate preparation. Using tricine gel electrophoresis to distinguish small size differences between proteins, we show that the NIR-OVASLP conjugate (approximately 3.5 kDa) does not contain any free NIRD1 dye (approximately 1 kDa including the Ahx linker) (**Figure 1a**). Subcutaneous injection in the flank is a common vaccination route in mice, which drains primarily to the inguinal lymph node in that flank. The proximity of injection site and draining lymph node likely hampers their distinction by optical imaging. As an alternative injection site, we injected NIR-OVASLP subcutaneously in the tail-base of a BALB/c nude mouse. This mouse strain is immunodeficient, but ideal for optical imaging due to the complete absence of hair and pigment. Within minutes after injection in the tail-base, lymph drainage towards the inguinal lymph node was clearly visible by live NIR fluorescence imaging (**Figure 1b**). The signal beyond the inguinal lymph node suggests further lymph transport by efferent vessels towards the axillary lymph node, as has been described before (28). We therefore injected B6 mice with NIR-OVASLP in the central tail-base and harvested inguinal and axillary lymph nodes from both flanks 90 minutes after injection, and quantified the NIR fluorescence signal.

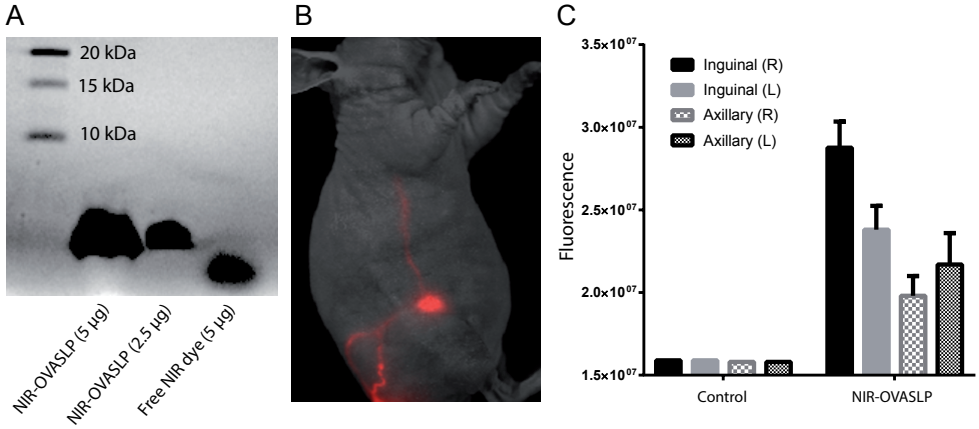

Figure 1. Inguinal and axillary lymph nodes drain the tail-base vaccination site. (A) Tricine gel electrophoresis of indicated amounts of NIRD1-labeled OVA24 SLP or free unbound NIRD1 dye, showing that the NIRD1-OVASLP conjugate does not contain unbound NIRD1 dye. The smallest three bands of a standard protein ladder are shown in the top. **(B)** NIR Fluorescence image of a BALB/c nude mouse 5 minutes after subcutaneous injection of NIR-OVASLP in the tail-base (not visible), and the drainage by the inguinal lymph node. **(C)** Measurement of NIR fluorescence in the left (L) and right (R) inguinal and axillary lymph nodes harvested from C57BL/6 mice 90 minutes after injection of NIR-OVASLP s.c. in the tail-base. Y-axis show the mean and SEM of the total radiant efficiency expressed in (photons/second) / ($\mu W/cm^2$). Lymph nodes from non-injected control mice are included as controls.

Injection in the tail-base results in vaccine accumulation primarily in the inguinal lymph nodes, whereas axillary lymph nodes showed lower fluorescence (**Figure 1c**). In summary, using a protocol of subcutaneous injection in the tail-base, we visualize drainage of SLP vaccines via lymphatic vessels to lymph nodes.

Fluorescence imaging of peptide vaccine kinetics

Our results show that the NIR-OVASLP construct can be visualized in draining lymph nodes by live imaging. Next, we analyzed whether NIRD1-labeling is sufficiently sensitive to visualize differential vaccine kinetics. We formulated the labeled vaccine in PBS, which is drained from the injection site rapidly, or in water-in-oil formulations using the mineral oil Montanide, which is used as a sustained-release formulation. Whereas clinical use of Montanide applies syringe extrusion as an emulsification method, preclinical studies most commonly mix the water and oil phase by vortex, which in general produces less stable emulsions with larger droplets (29,30). After subcutaneous injection of NIR-OVASLP in the tail-base of immunocompetent Albino B6 mice, NIR fluorescence imaging clearly identified the presence of the vaccine at the injection site (**Figure 2a**). To assess whether this NIR fluorescence-based vaccine tracking can be used to identify the kinetics of an administered vaccine, we formulated the NIR-OVASLP in three different ways: soluble peptide in saline (PBS), or 50/50 water-in-oil emulsions of the mineral oil Montanide emulsified either by Vortex or by Syringe Extrusion (SE). In order to follow the presence of the vaccine at the injection site and lymph nodes in time, we performed repeated measurements and quantified the NIR fluorescence signal in these areas of interest. The three formulations showed a clearly distinguishable pattern of clearance of the vaccine at the injection site, as shown by the drop in the fluorescent signal (**Figure 2b**). Corresponding with the expected pharmacokinetics of the different formulations, soluble SLP in PBS showed the fastest drop in fluorescent signal at the injection site. Interestingly, the SE formulation of Montanide-SLP showed a longer presence of peptide at the injection site than the exact same Montanide-SLP mixture prepared by Vortex. The NIR signal of Vortex-prepared emulsions at the injection site showed a two-phased pattern of a fast immediate drop followed by gradual decrease, consistent with heterogeneity in emulsion droplet size. Moreover, measurement of the flanks of the mice showed a clear NIR fluorescence signal in the vaccine-draining inguinal lymph nodes in the earliest days after injection (**Figure 2c,d**). The highest signal was found for the PBS free-peptide formulation, while the SE-formulated peptide was nearly undetectable in lymph nodes, and Vortex-formulated peptide showing an intermediate profile. Hence, a faster drop in fluorescence signal in the vaccination site corresponded with a higher signal in the lymph nodes, suggesting that our NIR fluorescence imaging protocol successfully quantified SLP drainage from the vaccination site to lymph nodes. In summary, these data show

the feasibility of SLP tracking by using NIR-labeled peptides. This imaging protocol allowed vaccine quantification at the injection site and visualization of lymph drainage, with sufficient sensitivity to distinguish vaccine formulations with distinct kinetics. Brewer et al. used MRI of iron-labeled Montanide to show that the oil remains at the injection site while the peptide epitope content encapsulated in liposomes gradually disappeared (31). Although the peptide length and formulation are different, this confirms the gradual release of peptide from Montanide depots as we visualized by NIR fluorescence imaging, a considerably less laborious and more subject-friendly technique compared to MRI (32).

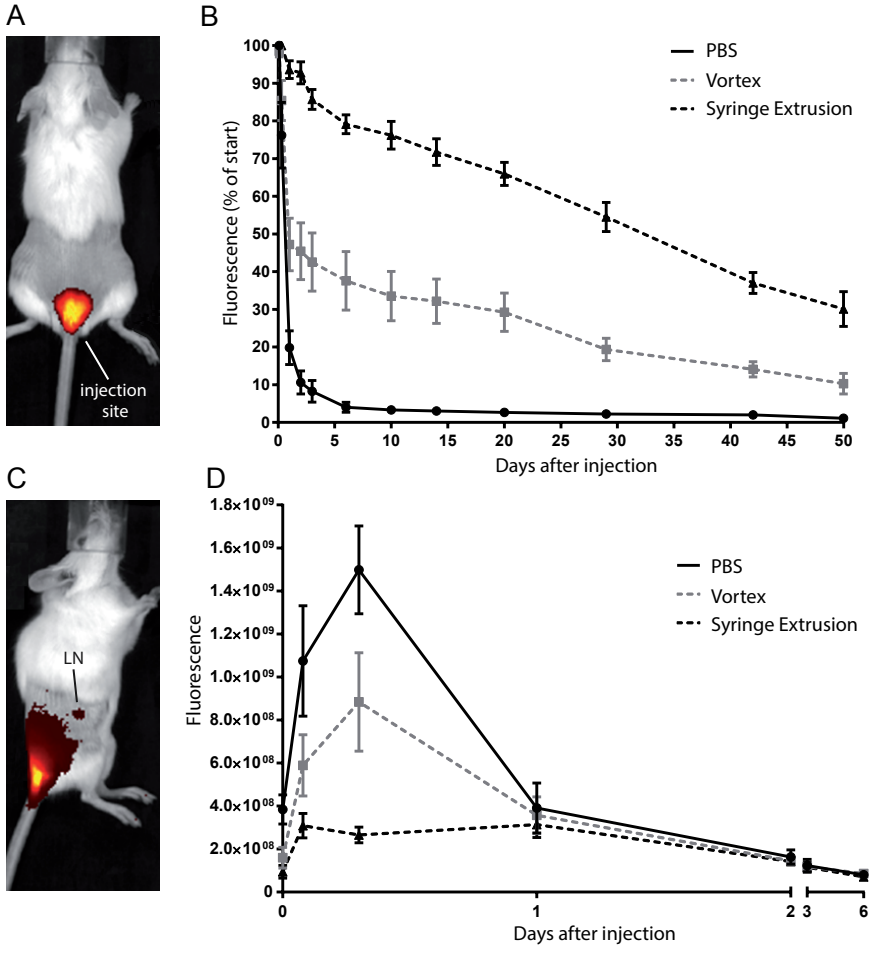

Figure 2. Visualization of peptide vaccine kinetics by fluorescence imaging. Examples of NIR-OVASLP fluorescence at the tail-base injection site (A) and the vaccine-draining inguinal lymph node (C) after injection in PBS. Quantification of vaccine fluorescence at the injection site (B) and vaccine-draining inguinal lymph nodes (D) of NIR-OVASLP formulated in PBS or in Montanide emulsions prepared by Vortex or Syringe Extrusion, as indicated. Fixed-size region of interest were used to quantify fluorescence, expressed as Total Radiant Efficiency in (photons/second) / (μW/cm²). The Y-axis shows the fluorescence signal either as a percentage of the starting signal after injection (B) or in absolute numbers (D).

SLP labeling does not hamper vaccine functionality

The validity of vaccine tracking using conjugated NIR dyes depends on the degree to which the presence of the dye affects the functional properties of the SLP vaccine. For instance, fluorescent and radioactive labeling of proteins and antibodies can significantly hamper the functional activity of the molecule of interest (33–35). To analyze whether NIRD1 conjugation hampered the immunogenicity of the SLP, we incubated D1 dendritic cells with labeled or unlabeled OVASLP and added the OVA-specific CD8 T cell hybridoma B3Z. T cell receptor (TCR) signaling in B3Z cells results in expression of the beta-galactosidase reporter as a measure of antigen presentation by dendritic cells and of vaccine functionality as such. The presence of NIRD1 on the OVASLP results in equal antigen processing and presentation as the unlabeled OVASLP (**Figure 3a**).

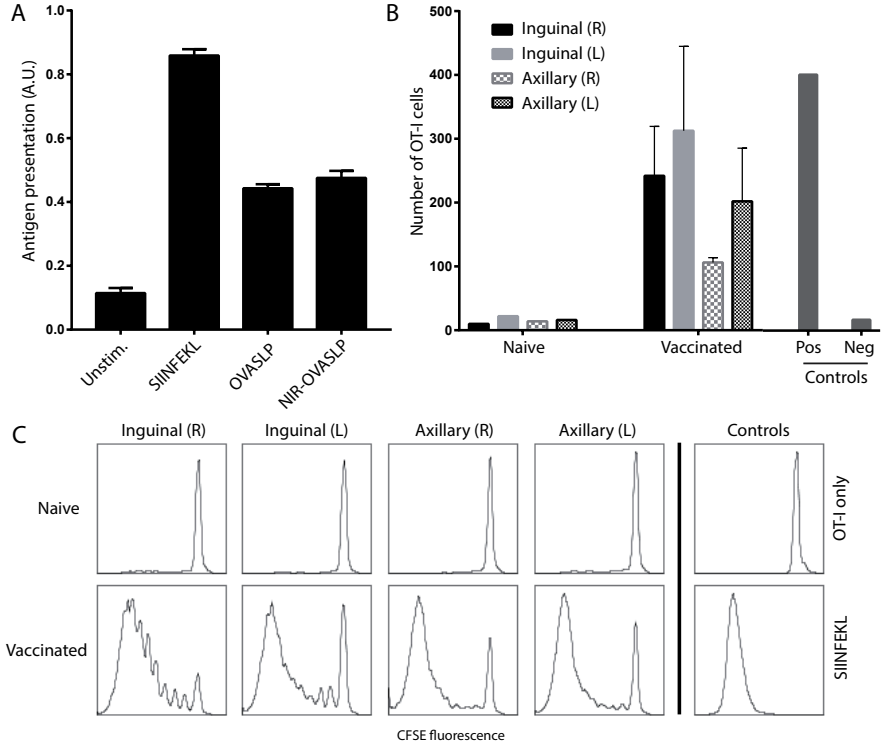

Figure 3. SLP labeling does not hamper vaccine functionality. (A) In vitro antigen presentation assay using OVA-specific B3Z CD8 T cell reporter cells. NIRD1-labeled or unlabeled OVA SLP was added to D1 dendritic cells and incubated overnight, followed by addition of B3Z cells. Presentation of the SIINFEKL epitope of OVA by dendritic cells to B3Z cells induces T cell receptor downstream signaling resulting in beta-galactosidase production, which enables a colorimetric assay as a measure of antigen presentation. Addition of SIINFEKL minimal epitope was used as positive control, non-incubated dendritic cells as negative control. **(B)** Proliferation of OT-I CD8 T cells incubated 4 days with single-cell suspensions of inguinal or axillary lymph nodes isolated from mice 90 minutes after vaccination with NIR-OVASLP in PBS the tail-base. The Y-axis shows the OT-I cell count normalized per 100 beads. Addition of SIINFEKL minimal epitope to a mixture of lymph node cells was used as positive control, OT-I cells not incubated with any lymph node cells or peptide served as negative control. **(C)** Visualization of OT-I cell proliferation from Figure 3B by showing CFSE fluorescence. Prior to incubation, OT-I cells were labeled with CFSE, which is distributed between daughter cells during proliferation, reducing CFSE fluorescence intensity per cell.

The superior result of the minimal peptide epitope SIINFEKL shows that B3Z activation functions in the absence of co-stimulatory signals. To assure NIR-OVASLP vaccine functionality in vivo, we mashed the tail-base vaccine-draining lymph nodes from Figure 1c and incubated them 4 days with OT-I cells, which are SIINFEKL-specific CD8 T cells isolated from a TCR-transgenic mouse. OT-I cells were pre-labeled with CFSE, a dye that is divided among daughter cells during proliferation and thereby allows visualization of T cell proliferation by the intensity of CFSE fluorescence in flow cytometry. OT-I cells incubated with vaccine-draining lymph nodes accumulated to much higher numbers than OT-I cells incubated with lymph nodes of naïve mice, or without lymph nodes (**Figure 3b**). FACS measurement of CFSE fluorescence confirmed that OT-I cells had massively proliferated after vaccination, as shown by the presence of cells with reduced CFSE fluorescence (horizontal axis) as a result of dilution by proliferation (**Figure 3c**). These results indicate that the conjugated NIRD1 dye leaves SLP functionality fully intact in vitro and in vivo, which validates correlation studies between SLP imaging and vaccine functionality.

Differential vaccine kinetics reflect local but not systemic T cell responses

To assess whether the varying vaccine kinetics were reflected in the ability to induce systemic T cell responses, we vaccinated mice with NIR-OVASLP formulated in PBS or in Montanide emulsions prepared by either Vortex or SE. On day 0, 3 or 14 after vaccination, mice received an adoptive transfer of vaccine-specific T cell receptor-transgenic OT-I CD8 T cells. Three days after T cell transfer, vaccine-draining lymph nodes and spleens were harvested to analyze the expansion of OT-I T cells as a measure of vaccine-induced T cell priming. Both formulations of Montanide emulsions induced strong vaccine-specific T cell proliferation in vaccine-draining lymph nodes and in the spleen (**Figure 4**). The higher SLP accumulation in lymph nodes draining Vortex emulsions, as compared to SE emulsions, was reflected in slightly stronger local T cell proliferation in lymph nodes, whereas differences in the spleen were not statistically significant. As expected, the non-adjuvanted peptide vaccine in PBS induced poor T cell proliferation due to the absence of T cell co-stimulation, despite the high levels of SLP in the lymph nodes after vaccination. This finding underscores the well-established important role of Montanide emulsions as vaccine adjuvants (11, 36). In conclusion, local differences in the presence of vaccine at the vaccination site and vaccine-draining lymph nodes are not necessarily reflected in the magnitude of systemic T cell responses. A previous study comparing different emulsions of a minimal peptide epitope vaccine in IFA, showed slightly lower T cell responses induced by Vortex-prepared vaccines when compared to Syringe Extrusion (37). We share their advice that vaccine emulsion protocols should be standardized to avoid large variability and undesired artefacts such as the inclusion of air bubbles in the emulsion, which favors the use of the Syringe Extrusion protocol.

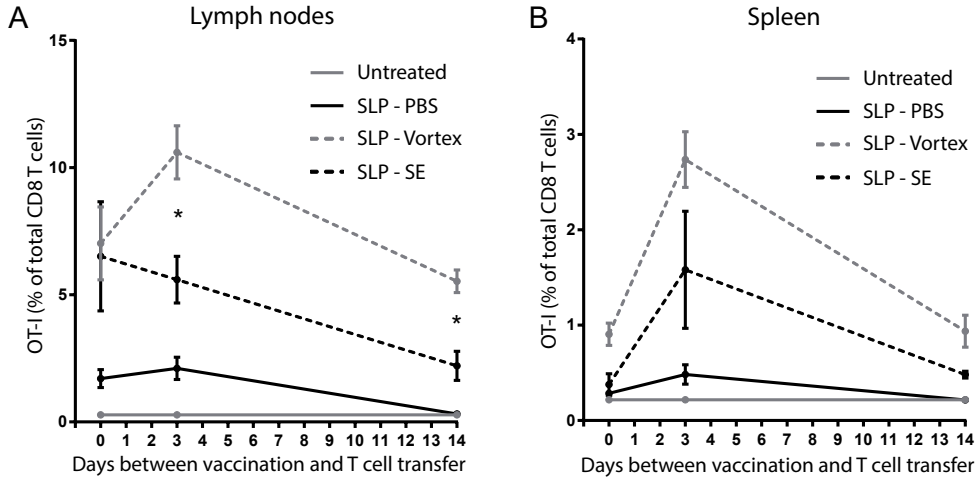

Figure 4. Differential vaccine kinetics reflect local but not systemic T cell responses. Expansion of vaccine-specific OT-I cells in vaccine-draining inguinal lymph nodes **(A)** and spleens **(B)** of mice 3 days after adoptive intravenous transfer of 1 million OT-I CD8 T cells. On day 0, 3 or 14 before OT-I transfer, mice were vaccinated in the tail-base with OVASLP formulated in PBS or in Montanide emulsions prepared by either Vortex or Syringe Extrusion (SE). Untreated naïve mice served as negative controls. The expansion of OT-I cells was quantified by flow cytometry and is presented as OT-I T cells as a percentage of total CD8 T cells. Statistically significant differences ($p<0.05$) by Student's t-test are indicated by asterisks (SLP-Vortex vs SLP-SE).

In summary, we show the feasibility of live NIR fluorescence SLP visualization and quantification at the injection site and in draining lymph nodes, and correlate vaccine kinetics to functionality in terms of T cell. We show that vaccine tracking can identify differences between vaccine formulations with varying kinetics. This does not exclude that besides the formulation, the characteristics of the peptide itself also influence vaccine kinetics (38). This issue can be addressed by comparing peptides with different lengths and physicochemical properties. Our NIRD1-based live fluorescence imaging platform serves as a useful tool to investigate fundamental and applied scientific questions in the field of vaccinology.

References

1. Castle JC, Loewer M, Boegel S, de Graaf J, Bender C, Tadmor AD, et al. Immunomic, genomic and transcriptomic characterization of CT26 colorectal carcinoma. BMC Genomics. 2014;15:190.
2. Yadav M, Jhunjhunwala S, Phung QT, Lupardus P, Tanguay J, Bumbaca S, et al. Predicting immunogenic tumour mutations by combining mass spectrometry and exome sequencing. Nature. 2014;515:572–6.
3. Kreiter S, Vormehr M, van de Roemer N, Diken M, Löwer M, Diekmann J, et al. Mutant MHC class II epitopes drive therapeutic immune responses to cancer. Nature. 2015;520:692–6.
4. Alexandrov LB, Nik-Zainal S, Wedge DC, Aparicio SAJR, Behjati S, Biankin A V, et al. Signatures of mutational processes in human cancer. Nature. 2013;500:415–21.

5. Van Allen EM, Miao D, Schilling B, Shukla SA, Blank C, Zimmer L, et al. Genomic correlates of response to CTLA-4 blockade in metastatic melanoma. Science. 2015;350:207–11.
6. Rizvi NA, Hellmann MD, Snyder A, Kvistborg P, Makarov V, Havel JJ, et al. Mutational landscape determines sensitivity to PD-1 blockade in non-small cell lung cancer. Science. 2015;348:124–8.
7. Topalian SL, Hodi FS, Brahmer JR, Gettinger SN, Smith DC, McDermott DF, et al. Safety, Activity, and Immune Correlates of Anti–PD-1 Antibody in Cancer. N Engl J Med. 2012;366:2443–54.
8. Hodi FS, O'Day SJ, McDermott DF, Weber RW, Sosman JA, Haanen JB, et al. Improved survival with ipilimumab in patients with metastatic melanoma. N Engl J Med. 2010;363:711–23.
9. Topalian SL, Drake CG, Pardoll DM. Immune Checkpoint Blockade: A Common Denominator Approach to Cancer Therapy. Cancer Cell. 2015;27:450–61.
10. Melief CJM, van der Burg SH. Immunotherapy of established (pre)malignant disease by synthetic long peptide vaccines. Nat Rev Cancer. 2008;8:351–60.
11. Slingluff CL. The present and future of peptide vaccines for cancer: single or multiple, long or short, alone or in combination? Cancer J. 2011;17:343–50.
12. Gubin MM, Zhang X, Schuster H, Caron E, Ward JP, Noguchi T, et al. Checkpoint blockade cancer immunotherapy targets tumour-specific mutant antigens. Nature. 2014;515:577–81.
13. Castle JC, Kreiter S, Diekmann J, Lower M, van de Roemer N, de Graaf J, et al. Exploiting the Mutanome for Tumor Vaccination. Cancer Res. 2012;72:1081–91.
14. Zwaveling S, Ferreira Mota SC, Nouta J, Johnson M, Lipford GB, Offringa R, et al. Established human papillomavirus type 16-expressing tumors are effectively eradicated following vaccination with long peptides. J Immunol. 2002;169:350–8.
15. Kenter GG, Welters MJP, Valentijn ARPM, Lowik MJG, Berends-van der Meer DMA, Vloon APG, et al. Vaccination against HPV-16 oncoproteins for vulvar intraepithelial neoplasia. N Engl J Med. 2009;361:1838–47.
16. Kenter GG, Welters MJP, Valentijn ARPM, Lowik MJG, Berends-van der Meer DMA, Vloon APG, et al. Phase I immunotherapeutic trial with long peptides spanning the E6 and E7 sequences of high-risk human papillomavirus 16 in end-stage cervical cancer patients shows low toxicity and robust immunogenicity. Clin Cancer Res. 2008;14:169–77.
17. van Poelgeest MIE, Welters MJP, van Esch EMG, Stynenbosch LFM, Kerpershoek G, van Persijn van Meerten EL, et al. HPV16 synthetic long peptide (HPV16-SLP) vaccination therapy of patients with advanced or recurrent HPV16-induced gynecological carcinoma, a phase II trial. J Transl Med. 2013;11:88.
18. van der Sluis TC, van Duikeren S, Huppelschoten S, Jordanova ES, Beyranvand Nejad E, Sloots A, et al. Vaccine-Induced Tumor Necrosis Factor-Producing T Cells Synergize with Cisplatin to Promote Tumor Cell Death. Clin Cancer Res. 2015;21:781–94.
19. Kleinovink JW, Van Driel PB, Snoeks TJ, Prokopi N, Fransen MF, Cruz LJ, et al. Combination of photodynamic therapy and specific immunotherapy efficiently eradicates established tumors. Clin Cancer Res. 2016;22:1459–68.
20. Etrych T, Lucas H, Janoušková O, Chytil P, Mueller T, Mäder K. Fluorescence optical imaging in anticancer drug delivery. J Control Release. 2016;226:168–81.
21. Leblond F, Davis SC, Valdés PA, Pogue BW. Pre-clinical whole-body fluorescence imaging: Review of instruments, methods and applications. J Photochem Photobiol B. 2010;98:77–94.
22. Vahrmeijer AL, Hutteman M, van der Vorst JR, van de Velde CJH, Frangioni J V. Image-guided cancer surgery using near-infrared fluorescence. Nat Rev Clin Oncol. 2013;10:507–18.
23. van Driel PBAA, van de Giessen M, Boonstra MC, Snoeks TJA, Keereweer S, Oliveira S, et al. Characterization and evaluation of the artemis camera for fluorescence-guided cancer surgery. Mol Imaging Biol. 2015;17:413–23.
24. Schaafsma BE, Mieog JSD, Hutteman M, van der Vorst JR, Kuppen PJK, Löwik CWGM, et al. The clinical use of indocyanine green as a near-infrared fluorescent contrast agent for image-guided oncologic surgery. J Surg Oncol. 2011;104:323–32.

25. Reinhart MB, Huntington CR, Blair LJ, Heniford BT, Augenstein VA. Indocyanine Green. Surg Innov. 2016;23:166–75.
26. Rahimian S, Kleinovink JW, Fransen MF, Mezzanotte L, Gold H, Wisse P, et al. Near-infrared labeled, ovalbumin loaded polymeric nanoparticles based on a hydrophilic polyester as model vaccine: Invivo tracking and evaluation of antigen-specific $CD8^+$ T cell immune response. Biomaterials. 2015;37.
27. Schägger H. Tricine–SDS-PAGE. Nat Protoc. 2006;1:16–22.
28. Harrell MI, Iritani BM, Ruddell A. Lymph node mapping in the mouse. J Immunol Methods. 2008;332:170–4.
29. Aucouturier J, Dupuis L, Deville S, Ascarateil S, Ganne V. Montanide ISA 720 and 51: a new generation of water in oil emulsions as adjuvants for human vaccines. Expert Rev Vaccines. 2002;1:111–8.
30. Fillmore PD, Brace M, Troutman SA, Blankenhorn EP, Diehl S, Rincon M, et al. Genetic analysis of the influence of neuroantigen-complete Freund's adjuvant emulsion structures on the sexual dimorphism and susceptibility to experimental allergic encephalomyelitis. Am J Pathol. 2003;163:1623–32.
31. Brewer KD, Lake K, Pelot N, Stanford MM, DeBay DR, Penwell A, et al. Clearance of depot vaccine SPIO-labeled antigen and substrate visualized using MRI. Vaccine. 2014;32:6956–62.
32. Kosaka N, Ogawa M, Choyke PL, Kobayashi H. Clinical implications of near-infrared fluorescence imaging in cancer. Future Oncol. 2009;5:1501–11.
33. Vira S, Mekhedov E, Humphrey G, Blank PS. Fluorescent-labeled antibodies: Balancing functionality and degree of labeling. Anal Biochem. 2010;402:146–50.
34. Gahlmann A, Moerner WE. Exploring bacterial cell biology with single-molecule tracking and super-resolution imaging. Nat Rev Microbiol. 2013;12:9–22.
35. Vergara I, Castillo E, Romero-Piña M, Torres-Viquez I, Paniagua D, Boyer L, et al. Biodistribution and Lymphatic Tracking of the Main Neurotoxin of Micrurus fulvius Venom by Molecular Imaging. Toxins. 2016;8:85.
36. Khong H, Overwijk WW. Adjuvants for peptide-based cancer vaccines. J Immunother Cancer. 2016;4:56.
37. Koh YT, Higgins SA, Weber JS, Kast WM. Immunological consequences of using three different clinical/laboratory techniques of emulsifying peptide-based vaccines in incomplete Freund's adjuvant. J Transl Med. 2006;4.
38. Weijzen S, Meredith SC, Velders MP, Elmishad AG, Schreiber H, Kast WM. Pharmacokinetic Differences Between a T Cell-Tolerizing and a T Cell-Activating Peptide. J Immunol. 2001;166.